UPR transducer BBF2H7 allows export of type II collagen in a cargo- and developmental stage–specific manner

Tokiro Ishikawa,[1] Takuya Toyama,[1] Yuki Nakamura,[1] Kentaro Tamada,[1] Hitomi Shimizu,[1] Satoshi Ninagawa,[1] Tetsuya Okada,[1] Yasuhiro Kamei,[2] Tomoko Ishikawa-Fujiwara,[3] Takeshi Todo,[3] Eriko Aoyama,[5] Masaharu Takigawa,[5] Akihiro Harada,[4] and Kazutoshi Mori[1]

[1]Department of Biophysics, Graduate School of Science, Kyoto University, Kyoto 606-8502, Japan
[2]Spectrography and Bioimaging Facility, National Institute for Basic Biology, Okazaki 444-8585, Japan
[3]Department of Radiation Biology and Medical Genetics and [4]Department of Cell Biology, Graduate School of Medicine, Osaka University, Suita 565-0871, Japan
[5]Advanced Research Center for Oral and Craniofacial Sciences, Okayama University Dental School/Graduate School of Medicine, Dentistry and Pharmaceutical Sciences, Okayama 700-8525, Japan

The unfolded protein response (UPR) handles unfolded/misfolded proteins accumulated in the endoplasmic reticulum (ER). However, it is unclear how vertebrates correctly use the total of ten UPR transducers. We have found that ER stress occurs physiologically during early embryonic development in medaka fish and that the smooth alignment of notochord cells requires ATF6 as a UPR transducer, which induces ER chaperones for folding of type VIII (short-chain) collagen. After secretion of hedgehog for tissue patterning, notochord cells differentiate into sheath cells, which synthesize type II collagen. In this study, we show that this vacuolization step requires both ATF6 and BBF2H7 as UPR transducers and that BBF2H7 regulates a complete set of genes (*Sec23/24/13/31*, *Tango1*, *Sedlin*, and *KLHL12*) essential for the enlargement of COPII vesicles to accommodate long-chain collagen for export, leading to the formation of the perinotochordal basement membrane. Thus, the most appropriate UPR transducer is activated to cope with the differing physiological ER stresses of different content types depending on developmental stage.

Introduction

The unfolded protein response (UPR) consists of translational and transcriptional programs. It is activated when the protein quality control system in the ER is compromised under a variety of physiological and pathological conditions, which are collectively termed ER stress. In this condition, translation is first generally and transiently suppressed to decrease the burden on the ER and then transcription is induced on genes encoding ER-localized molecular chaperones and folding enzymes (hereafter termed ER chaperones) and genes encoding components of ER-associated degradation, whose products aim to refold and degrade unfolded/misfolded proteins accumulated in the ER, respectively (Mori, 2000; Walter and Ron, 2011).

The critical importance of the UPR in the maintenance of homeostasis of the ER has been demonstrated by the identification of five mammalian UPR sensor/transducers, IRE1α, IRE1β, PERK, ATF6α, and ATF6β, and subsequent analysis of mice deficient in one or two of such transducers. *IRE1α*–single and *ATF6α/β*–double knockout (KO) cause embryonic lethality (Urano et al., 2000; Yamamoto et al., 2007), whereas *IRE1β*-KO mice show hypersensitivity to dextran sodium sulfate colitis (Bertolotti et al., 2001), and *PERK*-KO mice develop a diabetes milieu (Harding et al., 2001). Interestingly, mammals express a further five more ATF6-like ER membrane–bound transcription factors, which are also activated by regulated intramembrane proteolysis, namely OASIS/CREB3L1, BBF2H7/CREB3L2, Luman/LZIP/CREB3, CREB-H/CREB3L3, and AIbZIP/Tisp40/CREB3L4 (Fig. 1 A). Unlike ubiquitously expressed ATF6α and ATF6β, these factors often show tissue-specific expression (Asada et al., 2011). However, the question of why so many UPR transducers are required if ER stress means simply the accumulation of unfolded/misfolded proteins in the ER has remained unanswered.

We have started investigating what kind of protein or proteins cause ER stress physiologically during the early embryonic development of medaka fish, whose genome also contains genes coding for these ten UPR transducers (Ishikawa et al., 2011, 2013). Results have shown that ATF6α/β are responsible for transcriptional induction of ER chaperones in response to

Correspondence to Kazutoshi Mori: mori@upr.biophys.kyoto-u.ac.jp

Abbreviations used: CRE, cAMP-response element; dpf, d post fertilization; dph, d post hatch; KO, knockout; TILLING, targeting-induced local lesions in genomes; UPR, unfolded protein response; WT, wild type.

The Rockefeller University Press $30.00
J. Cell Biol. Vol. 216 No. 6 1761–1774
https://doi.org/10.1083/jcb.201609100

ER stress in medaka (Ishikawa et al., 2013) and in mice (Yamamoto et al., 2007), but these results are unlike to worms or flies, in which IRE1 is a major regulator of ER chaperone induction (Shen et al., 2005; Hollien and Weissman, 2006) as in yeast (Cox et al., 1993; Mori et al., 1993). We have further shown that *ATF6α/β*–double KO causes embryonic lethality in medaka as it does in mice and that *ATF6α/β*–double KO medaka show a severe defect in development of the notochord, which serves as the body axis before formation of the vertebra (Ishikawa et al., 2013). Our morpholino-mediated knockdown and mRNA injection –mediated overexpression experiments have clearly shown that the synthesis of large amounts of extracellular matrix proteins, such as type VIII collagen, during smooth alignment of the disk-like notochord cells is the cause of this physiological ER stress and that *ATF6α/β*–double KO medaka die because they cannot adjust levels of ER chaperones to meet these increased demands in notochord cells (Ishikawa et al., 2013).

It is well known that notochord cells secrete hedgehog to regulate patterning of various tissues such as neural tubes, somites, muscles, and the pancreas (Stemple, 2005). After patterning, a process called vacuolization begins, in which notochord cells differentiate into two cell types: a large vacuolated cell type, which plays a structural role in generating turgor in the notochord, and a thin nonvacuolated epithelial cell type (sheath cells), which starts to synthesize and secrete type II collagen upon receipt of Mib-Jag1-Notch signaling, leading to the formation of the perinotochordal basement membrane. Both vacuoles and the basement membrane are critical for the notochord to function as an early axial skeleton (Yamamoto et al., 2010).

A major difference between type VIII and type II collagen lies in their lengths (Fig. S1). Type II collagen is ∼1,500 aa long and contains 360 contiguous repeats of the triplet amino acids Gly-X-Y. In contrast, type VIII collagen is a short-chain collagen only about half the size of type II collagen (∼700 aa). In addition, because type VIII collagen has multiple breaks consisting of two amino acids within 145 repeats of the triplet amino acids Gly-X-Y, type VIII collagen can be folded into a compact structure and therefore can be incorporated into standard COPII vesicles (60–80 nm in diameter) for export from the ER. In marked contrast, the long rodlike structure (300–400 nm diameter) of type II collagen prevents its incorporation into standard COPII vesicles. COPII vesicles must be enlarged to accommodate type II collagen for export from the ER (Fig. 9; Malhotra and Erlmann, 2015).

COPII vesicles are covered by two layers of protein complex, namely an inner coat consisting of Sec23 and Sec24 (composed of Sec23a, Sec23b, Sec24a, Sec24b, Sec24c, and Sec24d in vertebrates) and an outer coat consisting of Sec13 and Sec31 (composed of sec13 alone, sec31a, and sec31b in vertebrates). Completion of the outer coat layer results in the budding of vesicles, as the Sec13–Sec31 complex has a curved structure. Recently, three mechanisms have been proposed to explain the enlargement of COPII vesicles to accommodate long-chain collagen. First, Tango1 delays the formation of the outer coat layer by simultaneously binding to long-chain collagen and Sec23/Sec24 proteins of the inner coat via the SH3 domain present at its N terminus and the proline-rich domain present at its C terminus, respectively (Saito et al., 2009b). Tango1-like proteins containing the proline-rich domain but lacking the SH3 domain, such as cTAGE5, heterodimerize with Tango1, which also helps delay the formation of the outer coat layer (Saito et al., 2011). Second, Tango1 recruits Sedlin, which promotes Sec23-mediated conversion of Sar1-GTP to Sar1-GDP; because Sar1-GTP causes membrane constriction, the presence of too much Sar1-GTP has a negative effect on enlargement (Venditti et al., 2012). Third, the ubiquitin ligase CUL3 (E3), only when coupled with its adapter molecule KLHL12 (Jin et al., 2012) and the two calcium-binding proteins PEF1 and ALG2 (McGourty et al., 2016), recognizes and monoubiquitinates Sec31, which is required for the formation of enlarged COPII vesicles.

We show in this study that the UPR transducer BBF2H7 (Fig. 1 B), one of the five ATF6-like ER membrane–bound transcription factors, plays a specific role in the process of notochord vacuolization via the transcriptional regulation of a complete set of genes essential for the enlargement of COPII vesicles, which is required for the export of type II collagen from the ER. It should be noted that BBF2H7 is synthesized as a type II transmembrane protein in the ER and that its N-terminal fragment BBF2H7(N), liberated from the membrane by ER stress–induced proteolysis in the Golgi apparatus, is translocated into the nucleus to activate transcription (Kondo et al., 2007).

Results

Phenotypes of *BBF2H7*-KO medaka

We used the targeting-induced local lesions in genomes (TILLING) method to identify *BBF2H7*-KO medaka and thereby amplified exon 1 of the *BBF2H7* gene from the mutant library with specific primers designed using information provided by the Ensemble Genome Browser (Hubbard et al., 2002). Among 5,760 male mutant fishes screened, we obtained a missense mutation (M1V) that changed the initiation codon ATG to GTG (Fig. 1 C). In this mutant allele, translation must start from the next ATG codon, resulting in a frame shift at the positions of D45 and A46 (Fig. 1 C). Thus, this mutant allele would not produce functional BBF2H7. In vitro fertilization and subsequent backcrossing against wild-type (WT) female fish yielded *BBF2H7* heterozygotes (N3). When *BBF2H7* heterozygotes (N3) were in crossed WT fish, heterozygotes and homozygotes were hatched with expected Mendelian ratios (Fig. 1 D). However, no *BBF2H7* homozygotes survived at 60 d post hatch (dph), although they were fed normally (Fig. 1 E). We also found that all WT fish survived even in the absence of feeding for 8 dph, whereas *BBF2H7* homozygotes started to die even at 1 dph, and the number of survivors kept decreasing until 8 dph (Fig. 1 F). These results indicated that deletion of *BBF2H7* did not cause embryonic lethality but conferred lethality after birth.

All *BBF2H7*-KO medaka showed two major apparent phenotypes at birth (Fig. 2 A), namely a flattened head (Fig. 2 B) and short tail (Fig. 2 E). Alcian blue staining confirmed the normal presence of all cartilage components of the skull, but the skull did not develop properly compared with WT medaka (Fig. 2 C). Alizarin red staining also showed incomplete bone formation (Fig. 2 D). Craniofacial abnormality in *BBF2H7*-KO medaka is consistent with previous studies showing that *BBF2H7*-KO mice show a severe defect in chondrogenesis and die by suffocation shortly after birth because of an immature short cavity (Saito et al., 2009a) and that the zebrafish *feelgood* mutant (carrying a point mutation in the DNA-binding domain of BBF2H7) exhibits a malfolded head skeleton (Melville et al., 2011). Therefore, we focused on the

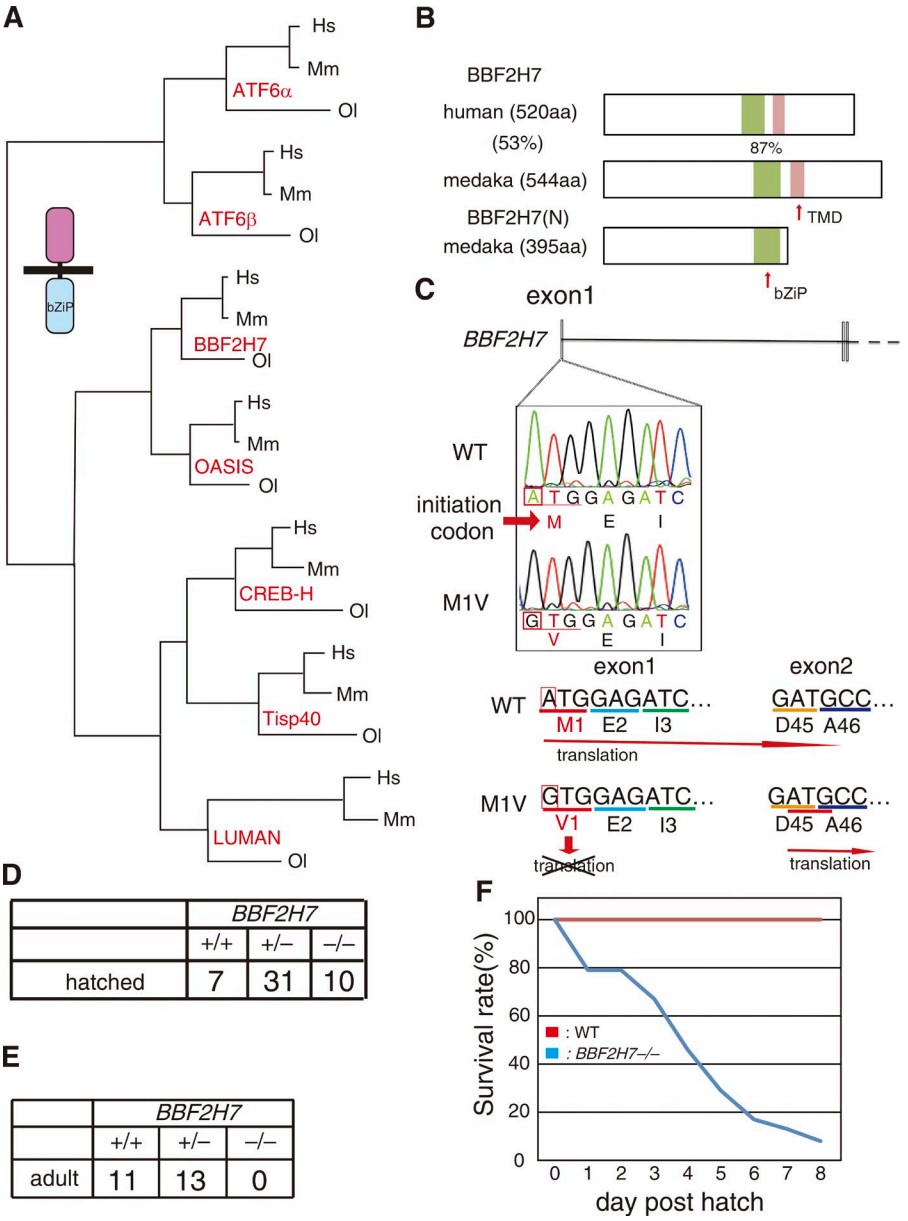

Figure 1. **Effect of deleting *BBF2H7* on medaka development.** (A) Phylogenic tree of ATF6α/β and five ATF6-like ER membrane–bound transcription factors inferred by the Whelan and Goldman (WAG) method using their full-length amino acid sequences. Hs, *Homo sapiens*; Mm, *Mus musculus*; Ol, *Oryzias latipes*. (B) Schematic structures of human and medaka BBF2H7 (full length) as well as the active form of BBF2H7, BBF2H7(N), and their identity at the amino acid level. bZIP and TMD denote the basic leucine zipper and transmembrane domain, respectively. (C) Missense mutation of BBF2H7 obtained by the TILLING method. The M1V mutation causes a frame shift at D45 and A46 as indicated. A, alanine; D, aspartic acid; E, glutamate; I, isoleucine; M, methionine; V, valine. (D) *BBF2H7* heterozygotes were in-crossed, and the resulting 48 hatched fish were genotyped. (E) *BBF2H7* heterozygotes were in-crossed, and hatched fish were grown under normal feeding conditions. The 24 fish that survived until 60 dph were then genotyped. (F) *BBF2H7* heterozygotes were in-crossed, and hatched fish were grown under nonfeeding conditions. Dead fish were genotyped.

short-tail phenotype because the shortening was much more severe in *BBF2H7*-KO medaka (null mutant) than in the zebrafish *feelgood* (point) mutant.

We first asked from which stage the difference in tail length became evident. When the length from the pectoral fin to the caudal fin was measured, a significant difference between WT and *BBF2H7*-KO medaka was found to already exist at 3 d post fertilization (dpf) and kept increasing until 7 dpf, the time when the medaka hatched (Fig. 2 F). We determined the number of somites present from the posterior region of the pectoral fin to the caudal fin as well as the length of each somite in hatched fish. Results showed that although the number of somites did not significantly differ between the WT and *BBF2H7*-KO medaka (Fig. 2 G), the length of each somite in *BBF2H7*-KO medaka was nearly half that in WT medaka (Fig. 2 H). This suggested that the developmental program for differentiation of somites is not perturbed in *BBF2H7*-KO medaka but that the driving force for somite extension may be weak.

Compromised secretion of type II collagen in the notochord of *BBF2H7*-KO medaka

We next determined which cell types express BBF2H7 by creating a transgenic line in which Venus was expressed under the control of the *BBF2H7* promoter. To this end, the first exon of the *BBF2H7* gene was replaced with the gene encoding Venus in a fosmid vector containing a nearly 40-kb medaka genomic fragment, which was used as a transgene (P_{BBF2H7}-*Venus*; Fig. 3 A). We observed scant Venus expression at stage 19 (see Fig. 2 I for the relationship between dpf and stage in medaka), when both somites and the notochord started to form, but we observed weak Venus expression in the entire embryonic body from stage 21 (Fig. 3 B). At stages 24 and 25, Venus expression was clearly observed in disk-like notochord cells, whereas somites existing at both sides of the notochord expressed Venus very weakly (Fig. 3, B and C), suggesting that the short-tail phenotype of *BBF2H7*-KO medaka may be caused by a progression defect of the notochord. Indeed, the time course of notochord progression (Fig. 3 D) mirrored that of tail length (Fig. 2 F). Importantly,

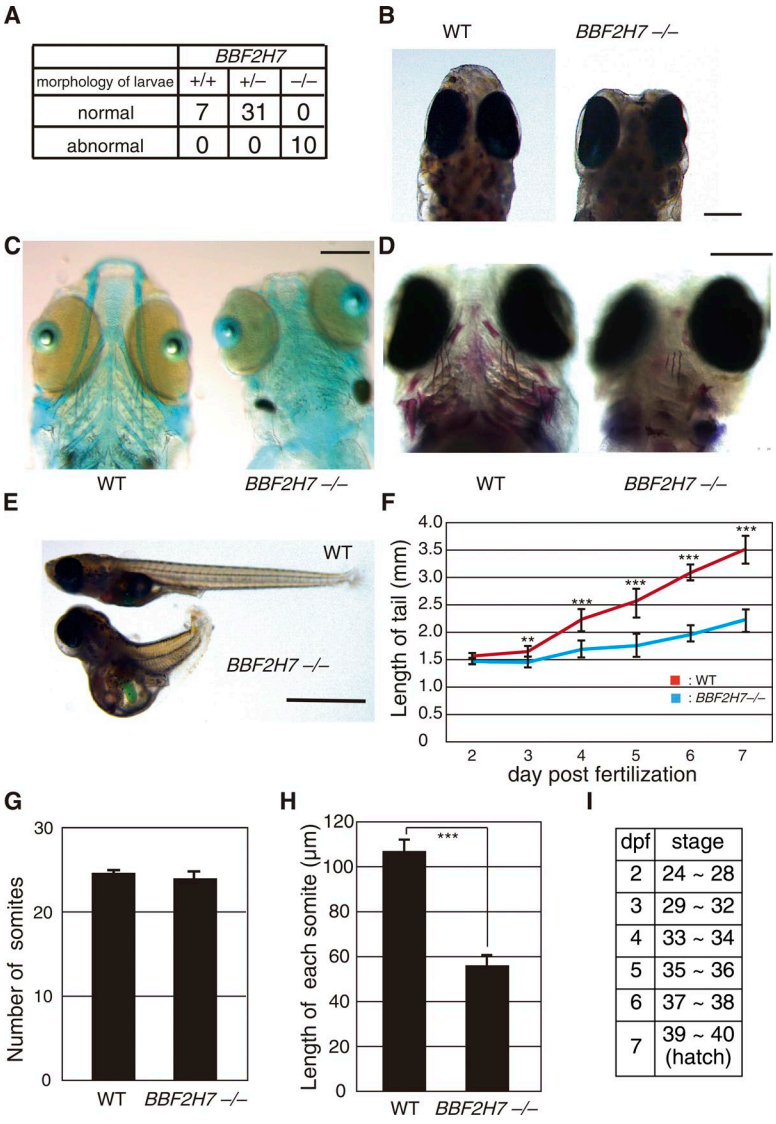

Figure 2. **Abnormal phenotypes of *BBF2H7*-KO medaka.** (A) Classification of morphology of hatched fish obtained in Fig. 1 D and its correlation with *BBF2H7* genotypes. (B) Craniofacial abnormality of *BBF2H7*-KO medaka compared with WT medaka at birth. (C) Alcian blue staining of the skulls of hatched WT and *BBF2H7*-KO medaka. (D) Alizarin red staining of the skulls of hatched WT and *BBF2H7*-KO medaka. (E) Tail shortening of *BBF2H7*-KO medaka compared with WT medaka at birth. Bars: (B–D) 250 µm; (E) 1 mm. (F) Difference in tail length between WT (n = 6) and *BBF2H7*-KO (n = 3 for 2–6 dpf; n = 2 for 7 dpf) medaka. (G) Difference in the number of somites between hatched WT and *BBF2H7*-KO medaka (n = 12). (H) Difference in somite lengths between hatched WT and *BBF2H7*-KO medaka (n = 12). Data presented are means ± SD. **, P < 0.01; ***, P < 0.001. (I) Relationship between dpf and developmental stage in medaka.

although we found no difference in the length of the notochord before stage 25 and therefore no difference in the smooth alignment of notochord cells between WT and *BBF2H7*-KO medaka, a significant difference in the length of the notochord was observed during the vacuolization step, which was initiated from the anterior part at stage 26, progressed toward the posterior part, and was completed by stage 33 (Fig. 3, C and D). At stage 36, there was nearly a twofold difference in notochord length between WT and *BBF2H7*-KO medaka (Fig. 3 E). This progression defect of the notochord may have caused the defect of somite extension in *BBF2H7*-KO medaka (Fig. 2 H). A coordination mechanism for the progression of notochord and somite development would be expected, given that both are important structural components of the tail. In this connection, it was previously shown that the notochord is required to initiate and maintain ventral identity in the somite (Dietrich et al., 1993).

We further found that vacuolated notochord was distorted multiple times in *BBF2H7*-KO medaka but not in WT medaka (Fig. 4 A). Venus expression from P_{BBF2H7}-*Venus* was lower in *BBF2H7*-KO medaka than in WT medaka, suggesting that BBF2H7 may enhance its own transcription. Interestingly, when we crossed *BBF2H7* heterozygotes with *ATF6α* heterozygotes or *ATF6β* heterozygotes carrying P_{BiP}-*EGFP*, which expresses EGFP under the control of the ER chaperone *BiP* promoter (Ishikawa et al., 2011), we observed more bending of vacuolated notochord in *BBF2H7*, *ATF6α*–double KO, and *BBF2H7 ATF6β*–double KO medaka than in single *BBF2H7*-KO medaka (Fig. 4, B and C). This indicates that the vacuolization step of notochord cells requires both functional ATF6 (ATF6α or ATF6β) and BBF2H7 as UPR transducers, unlike the smooth alignment step of notochord cells, which requires only functional ATF6 (ATF6α or ATF6β; Ishikawa et al., 2013).

Because Venus expression from P_{BBF2H7}-*Venus* clearly showed BBF2H7 expression in sheath cells but not in large vacuolated cells (Fig. 3 C; see Fig. 5 C for a schematic presentation of notochord structure), we focused on type II collagen, which is synthesized and secreted by sheath cells but not by large vacuolated cells. To improve notochord cell visualization, we created a transgenic line in which Venus is expressed under the control of the *brachyury* promoter (Fig. S2 A) similarly to the case of a transgenic line expressing P_{BBF2H7}-*Venus* described in Fig. 3 A; brachyury is highly expressed in the notochord of mice and zebrafish (Wilkinson et al., 1990; Schulte-Merker et al., 1992) as also in medaka (Fig. S2 B).

As shown in Fig. 4 D, smoothly aligned notochord cells synthesizing type VIII collagen (Ishikawa et al., 2013) were not

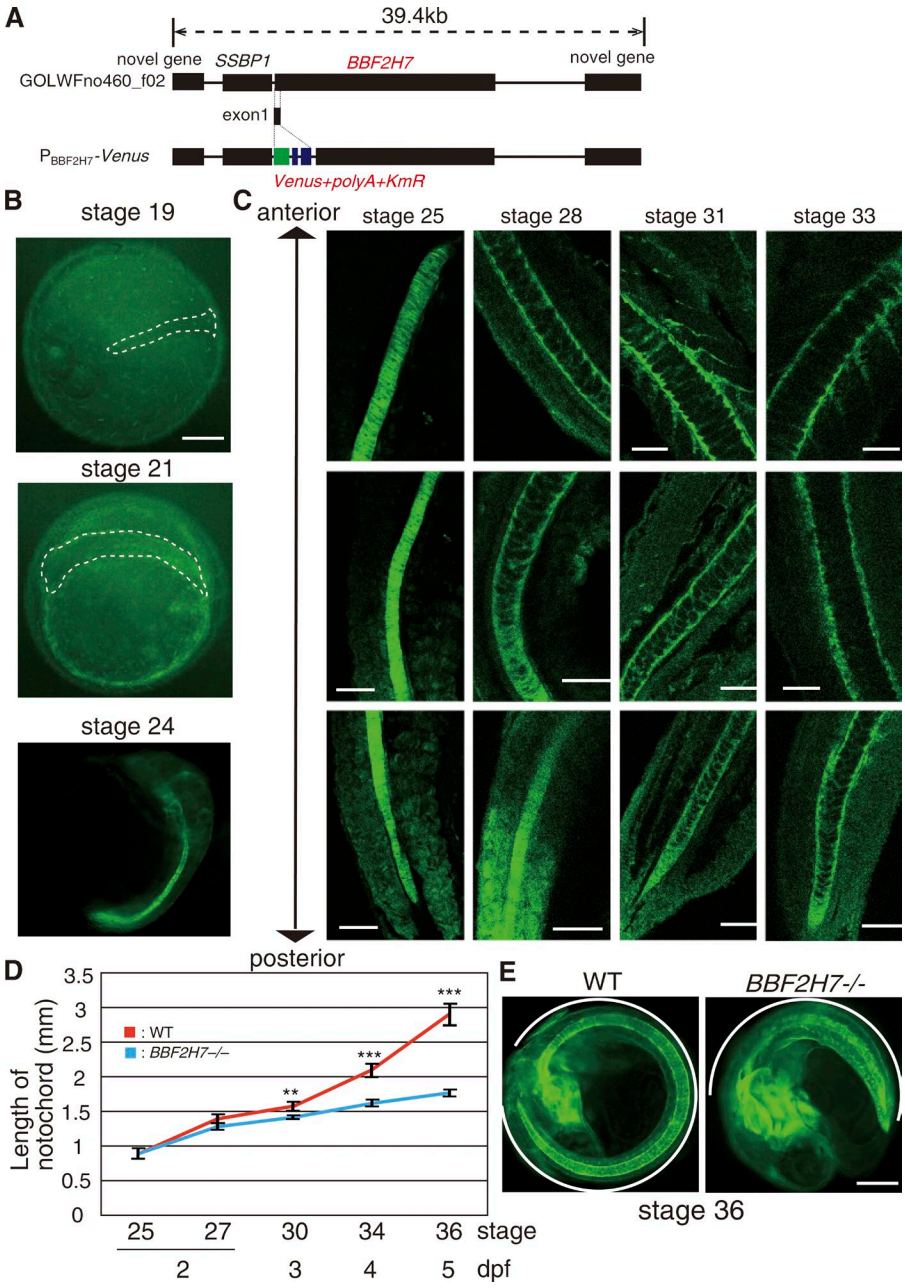

Figure 3. **Effect of deleting *BBF2H7* on the notochord.** (A) Schematic structures of the insert in the fosmid vector GOLWFno460_f02 and the construct, which was microinjected into one cell–stage embryos to create a transgenic line expressing Venus under the control of the *BBF2H7* promoter (P_{BBF2H7}-*Venus*). (B) Fluorescence microscopic analysis of WT medaka expressing P_{BBF2H7}-*Venus* at stages 19, 21, and 24. White dashed lines denote embryonic bodies. (C) Confocal microscopy visualizing of Venus expression in the notochord of WT medaka expressing P_{BBF2H7}-*Venus* at stages 25, 28, 31, and 33. (D) Difference in notochord length between WT and *BBF2H7*-KO medaka (n = 3). Data presented are means ± SD. **, $P < 0.01$; ***, $P < 0.001$. (E) Fluorescence microscopic analysis of WT and *BBF2H7*-KO medaka expressing P_{BBF2H7}-*Venus* at stage 36. White outlines point to notochords. Bars: (B and E) 250 µm; (C) 50 µm.

stained with anti–type II collagen antibody as expected (lower part of the notochord). The immunostaining clearly showed that the vacuolated notochord of both WT and *BBF2H7*-KO medaka started to synthesize type II collagen, indicative of the receipt of Mib-Jag1-Notch signaling (Fig. 4 D, white dashed boxes; see inset). Importantly, type II collagen was secreted into the extracellular space to cover the vacuolated notochord as a sheath (perinotochordal basement membrane) in WT medaka, whereas type II collagen remained punctate in *BBF2H7*-KO medaka (Fig. 4 D). This explains the bending of the uncovered notochord during vacuolization in *BBF2H7*-KO medaka and the subsequent failure of progression of the notochord.

We next determined where type II collagen is localized in the notochord of WT and *BBF2H7*-KO medaka by double immunostaining of the ER marker protein calnexin and type II collagen. In WT medaka, anticalnexin antibody clearly showed polarized localization of the ER in sheath cells, which was immediately covered by the perinotochordal basement membrane containing type II collagen (Fig. 5 A). Thus, the sheath cell–containing zone was separated from the vacuolated cell–containing zone, and calnexin-positive ER were distributed very closely to one side of the sheath cells, leading to extension of both the ER and perinotochordal basement membrane as adjacent straight lines (Fig. 5 A, WT; see particularly the merge inset) as shown previously in zebrafish (Yamamoto et al., 2010) and as schematically depicted in Fig. 5 C; vacuolated cells are surrounded by sheath cells, which are covered by the perinotochordal basement membrane. This may suggest that type II collagen secreted from the ER might reach the plasma membrane without passing through the Golgi apparatus.

In marked contrast, such polarized localization of the ER in sheath cells as well as separation of the sheath cell–containing zone from the vacuolated cell–containing zone was completely lost in the notochord of *BBF2H7*-KO me-

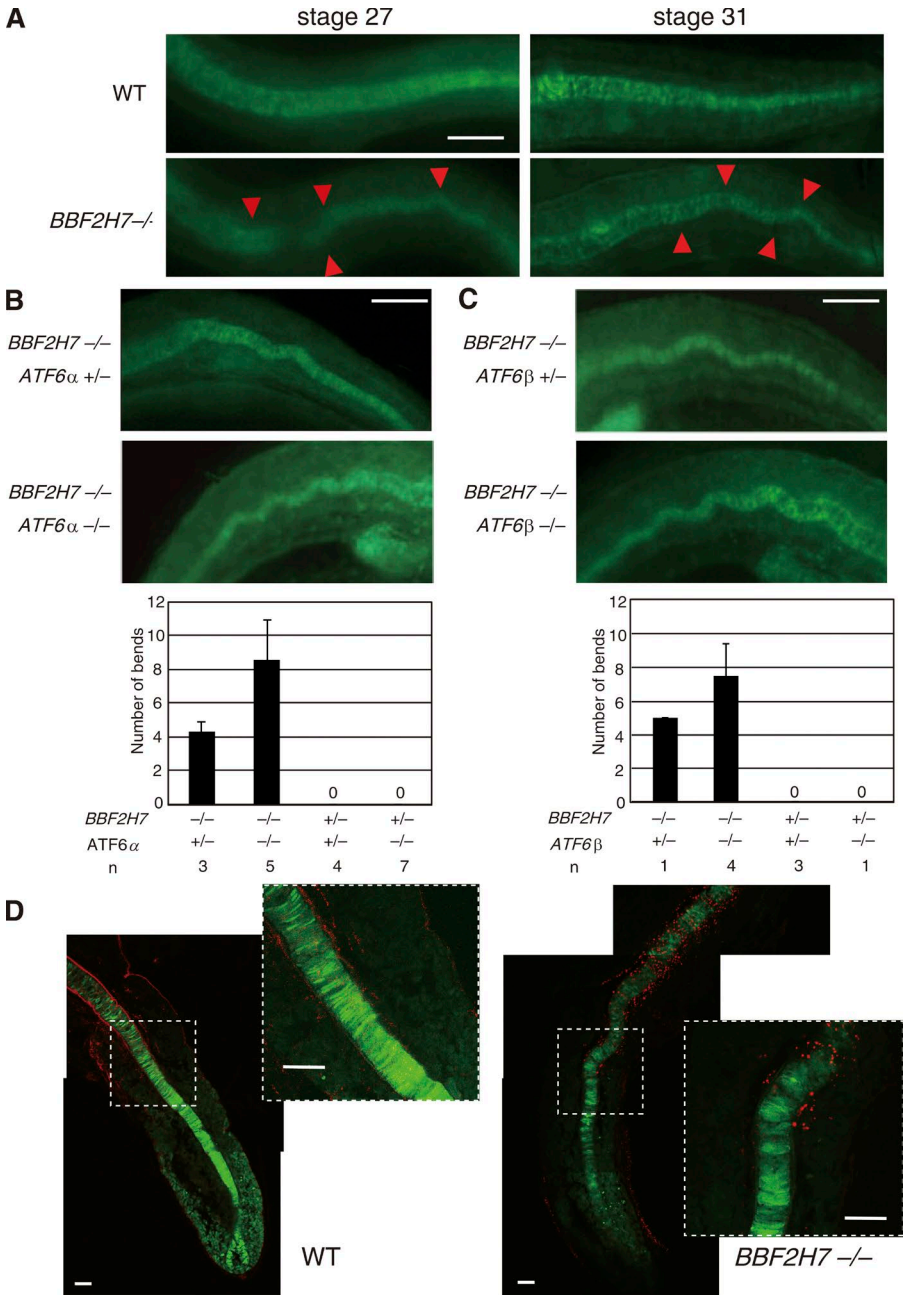

Figure 4. **Abnormal vacuolization of notochord cells in *BBF2H7*-KO medaka.** (A) Fluorescence microscopic analysis of WT and *BBF2H7*-KO medaka expressing P_{BBF2H7}-*Venus* at stages 27 and 31. Red arrowheads indicate bending sites. (B and C) *BBF2H7* heterozygotes were crossed with *ATF6α* (B) or *ATF6β* heterozygotes (C) carrying P_{BiP}-*EGFP*. The notochords of resulting fish with various genotypes were analyzed by a fluorescence microscope at stage 31 at the optimal exposure time (fluorescence intensity in $ATF6\alpha^{-/-}$ and $ATF6\beta^{-/-}$ was ~60 and 80%, respectively, of that in $ATF6\alpha^{+/-}$ or $ATF6\beta^{+/-}$ medaka). Entire notochords were photographed, and the numbers of observed bendings were counted, as shown at the bottom. Data presented are means ± SD. (D) Immunofluorescence analyses of notochords at stage 27 of WT and *BBF2H7*-KO medaka expressing $P_{brachyury}$-*Venus* using an anti–type II collagen antibody. Insets are denoted by white dashed boxes. These are composite images. Bars: (A–C) 100 µm; (D) 30 µm.

daka (Fig. 5 A). During vacuolization (Fig. 5 A, *BBF2H7*$^{-/-}$, bottom part of the notochord surrounded by the white dashed line; see particularly the "merge" inset) sheath cells and vacuolated cells were mixed, resulting in the staining of type II collagen–containing large aggregates at various places between two layers of the perinotochordal basement membrane. These large aggregates were most likely retained in the ER of sheath cells because calnexin-positive punctate structures surrounded (or at least attached to) those aggregates and because electron microscopy revealed the presence of many expanded ER with ribosomes in the notochord of *BBF2H7*-KO medaka but not in that of WT medaka (Fig. 6, ribosomes can be seen in the red dashed box after enlargement; see the left panel of *BBF2H7*$^{-/-}$). After completion of vacuolization, it appeared that large aggregate-containing sheath cells were detached from the notochord, as visualized in Fig. 5 B (some brachyury-positive cells were found outside of the notochord), resulting in the presence and absence of type II collagen–containing large aggregates outside and inside, respectively, the notochord (Fig. 5 A, *BBF2H7*$^{-/-}$, top part of the notochord in the yellow dashed box, which is enlarged in Fig. 5 D). The presence of these large aggregates outside of the notochord is the likely cause of apparently more profound red staining observed at the upper part, where vacuolization was completed, than that observed at the bending site, where vacuolization was in progress, in *BBF2H7*-KO medaka (Fig. 4 D). We concluded that BBF2H7 is required for secretion of type II collagen and proper formation of the perinotochordal basement membrane.

Transcriptional targets of BBF2H7

We then determined expression levels of various genes involved in the enlargement of COPII vesicles in embryos at stage 28 and notochords at stage 27 using quantitative RT-PCR. Results clearly showed that those genes involved in the formation of not

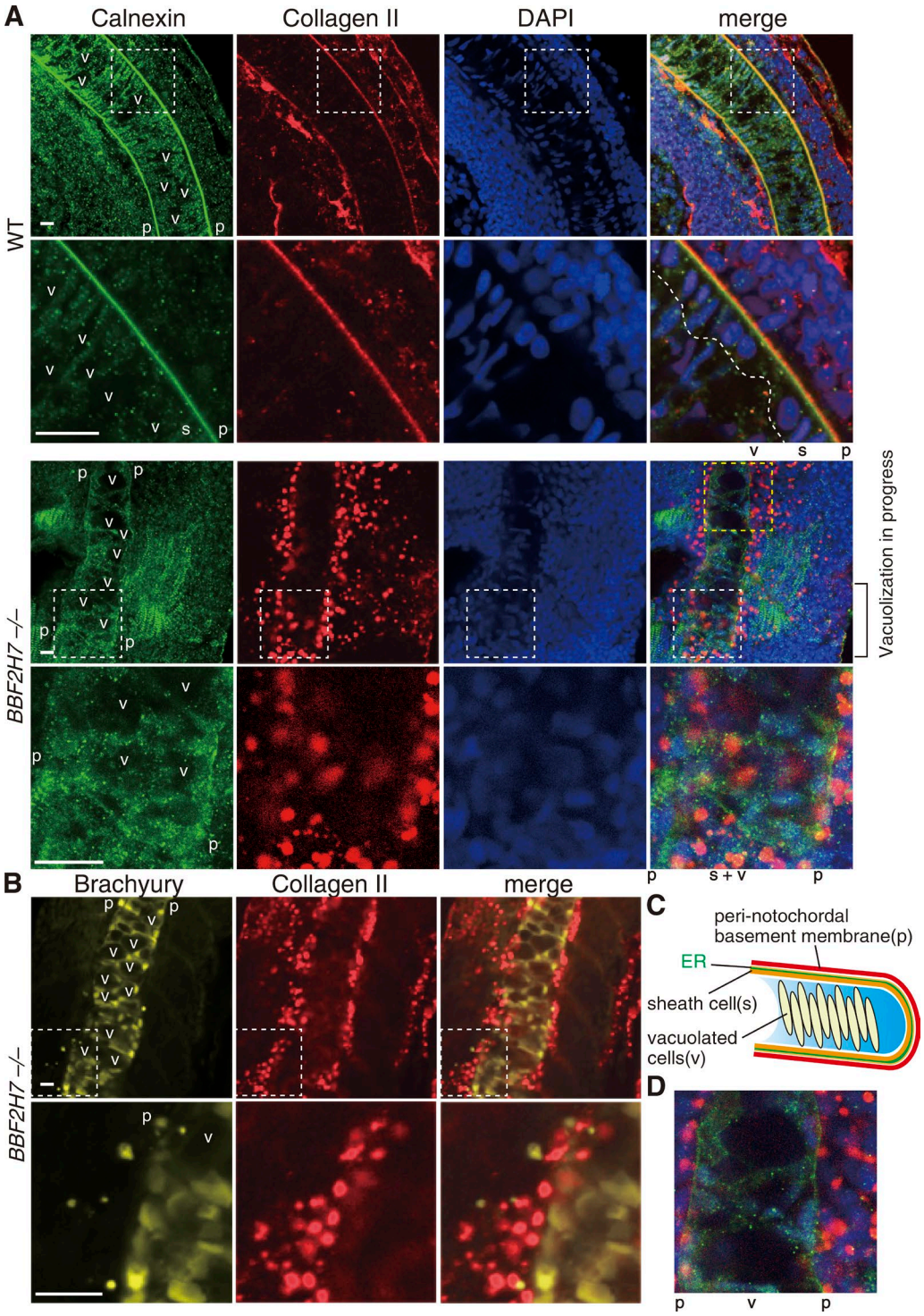

Figure 5. **Effect of deleting *BBF2H7* on formation of the perinotochordal basement membrane.** (A) Double immunofluorescence analysis of the notochord at stage 27 of WT and *BBF2H7*-KO medaka using anti-calnexin and anti–type II collagen antibodies as well as DAPI staining. Areas surrounded by the white dashed boxes are enlarged beneath each panel. The dashed line in the bottom right WT panel shows the separation of the sheath cell–containing zone (right) from the vacuolated cell–containing zone (left). (B) Immunofluorescence analysis using the anti–type II collagen antibody along with fluorescence microscopic analysis of an area of the notochord of *BBF2H7*-KO medaka carrying $P_{brachyury}$-*Venus* at stage 27, where the vacuolization was completed. Bars, 10 µm. (C) Schematic representation of notochord structure after vacuolization. (D) Enlarged area surrounded by the yellow dashed line in A. p, perinotochordal basement membrane; s, sheath cell; v, vacuolated cell. Scale is the same as other insets.

only the inner coat (*sec23a* and *sec24d*) but also the outer coat (*sec13* and *sec31a*) as well as genes essential for enlargement (*Tango1*, *Sedlin*, and *KLHL12*) are markedly down-regulated in the notochord of *BBF2H7*-KO medaka compared with WT medaka (Fig. 7 B) but not in whole embryos (Fig. 7 A and unpublished data). In addition to the three mechanisms described in the Introduction, it was previously shown that a cytoplasmic protein called SLY1 interacts with the cytoplasmic region of

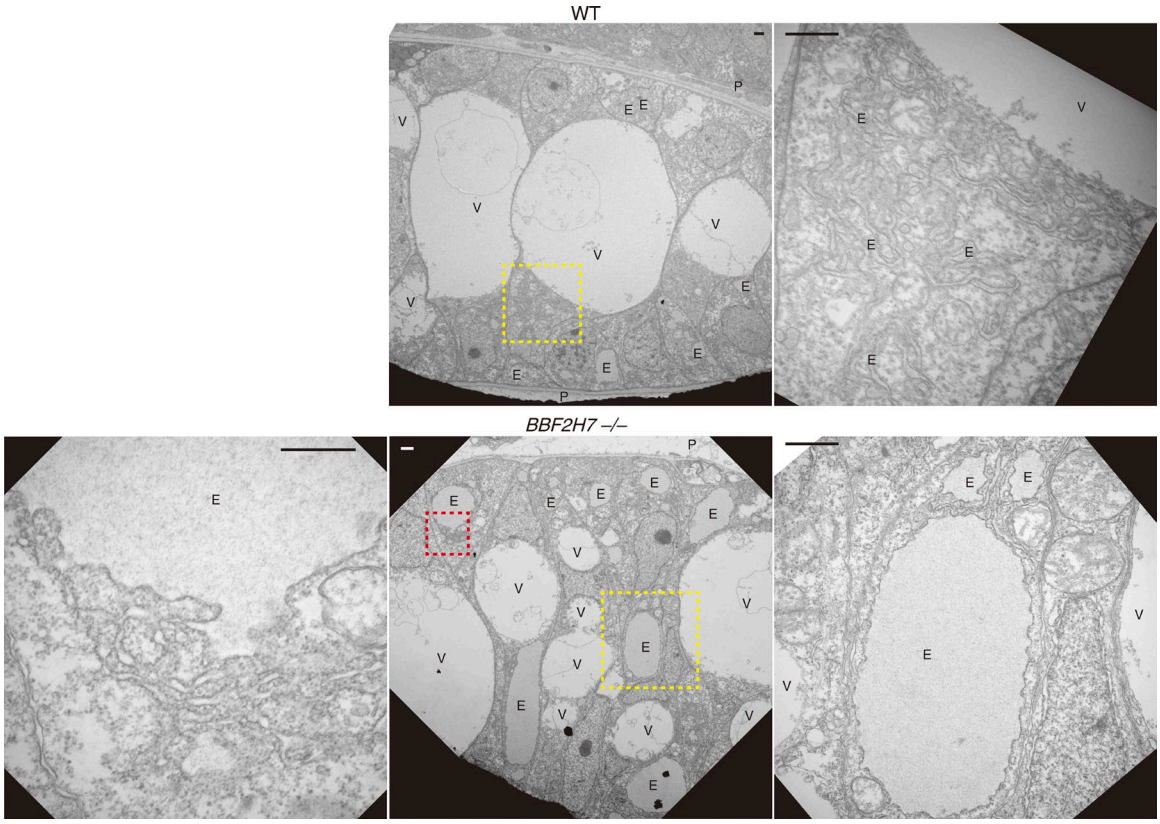

Figure 6. **Abnormal ER expansion in the notochord of *BBF2H7*-KO medaka.** Electron microscopic analysis of the notochord at stage 27 of WT and *BBF2H7*-KO medaka. Areas surrounded by the yellow and red dashed boxes are enlarged on the right and left, respectively. p, perinotochordal basement membrane; V, vacuole; E, ER. Bars are 1,000 nm except for the bottom left panel, which is 500 nm.

Tango1 and that SLY1 and Syntaxin 18, one of the ER-specific soluble NSF-attachment protein receptor (SNARE) proteins, are required for the export of type VII procollagen from the ER, although SLY1 can also interact with other ER-specific SNA RE proteins such as Syntaxin 5 and Syntaxin 17 (Nogueira et al., 2014). It was also shown that Rab10 is required for delivery of basement membrane proteins to the basal cell surface in addition to Tango1 (Lerner et al., 2013). Interestingly, we found among them that only *SLY1* mRNA was significantly down-regulated in the notochord of *BBF2H7*-KO medaka compared with WT medaka (Fig. 7 B).

In marked contrast, only the *Sec23a* and *Sec13* genes were significantly down-regulated in the notochord at stage 27 of *ATF6α/β*–double KO medaka compared with WT medaka (Fig. 7 C). Thus, BBF2H7 but not ATF6α/β is required for the expression of a complete set of genes involved in the formation of enlarged COPII vesicles. The level of *HSP47* mRNA encoding a collagen-specific molecular chaperone was not affected by *BBF2H7*-KO or *ATF6α/β*–double KO. Interestingly, levels of *Col2a1-1* mRNA and *Col2a1-2* mRNA, which both encode type II collagen, were not affected by *BBF2H7*-KO but were markedly down-regulated by *ATF6α/β*–double KO, suggesting that impairment of the smooth alignment of notochord cells in *ATF6α/β*–double KO medaka inhibited the receipt of Mib-Jag1-Notch signaling by sheath cells.

Importantly, mRNA injection-mediated transient overexpression of the full-length BBF2H7 rescued the abnormal (distorted notochord) phenotype in the embryo of *BBF2H7*-KO medaka, albeit only partially (Fig. 8 A). We also microinjected mRNA encoding BBF2H7(N), an active form of BBF2H7 that can translocate into the nucleus without ER stress–induced proteolysis (see Fig. 1 B); however, overexpression of BBF2H7(N) appeared to be extremely toxic, and no injected embryos reached stage 16, when the embryonic body is formed after gastrulation. We were therefore unable to examine how efficiently BBF2H7(N) rescues the defect in the notochord compared with the full-length BBF2H7. Instead, we examined the effect of transient overexpression of BBF2H7(N) in the transcription of genes in embryos at stage 15, and found significant up-regulation of mRNA encoding Sec23a, Sec24d, Sec13, Sec31a, and Tango1, but not Sedlin or KLHL12 (Fig. 8 B). Consistent results were obtained when the human chondrosarcoma-derived chondrocytic cell line HCS-2/8, which synthesizes and secretes a large amount of type II collagen, was transfected with human BBF2H7(N) (Fig. 8 C), but not when other cells, such as human colorectal carcinoma cell HCT116, were similarly transfected (Fig. S3; see Discussion for explanation).

We finally intended to determine whether BBF2H7 is directly involved in transcriptional up-regulation of the *Sec23a* and *Tango1* genes by constructing and injecting respective promoter–firefly luciferase genes with or without *BBF2H7(N)* mRNA at the one-cell embryo stage. Reporter assays conducted at stage 15 revealed that BBF2H7(N) markedly enhanced luciferase expression from both promoters (Fig. 8 D, WT), clearly indicating that the *Sec23a* and *Tango1* genes are direct transcriptional targets of BBF2H7. In mice, it was previously shown that the cAMP-response element (CRE)-like sequence TAACGTAA (-805 to -798; transcriptional start site

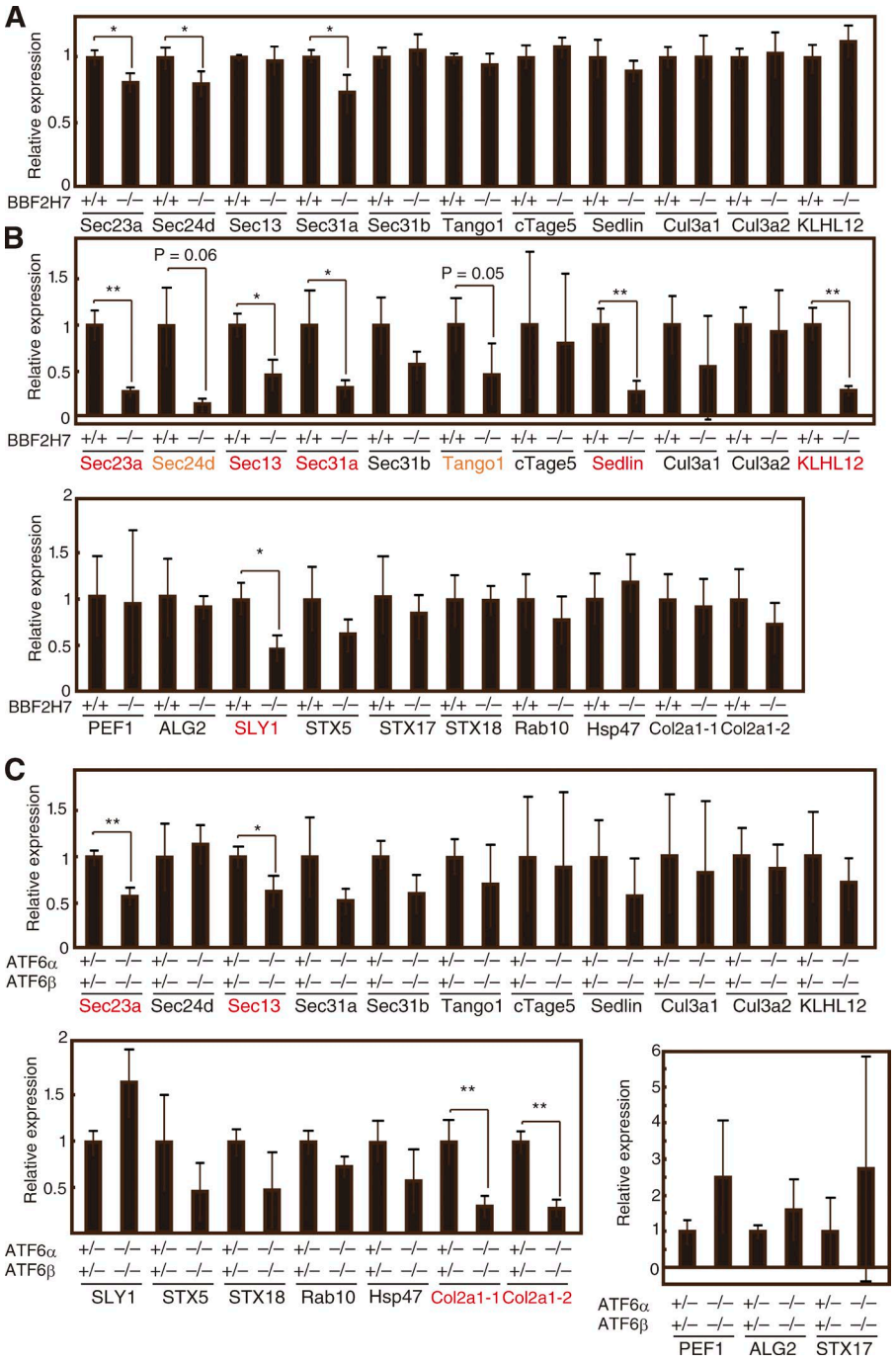

Figure 7. **Effect of deleting *BBF2H7* or *ATF6α/β* on expression of genes involved in the formation of enlarged COPII vesicles.** (A and B) Quantitative RT-PCR analysis of expression levels of genes involved in the formation of enlarged COPII vesicles in embryos at stage 28 (A) or notochord at stage 27 (B) of WT (+/+) and *BBF2H7*-KO(−/−) medaka relative to the expression level of β-actin (n = 3). (C) Quantitative RT-PCR analysis of expression levels of genes involved in the formation of enlarged COPII vesicles in notochords at stage 27 of *ATF6α/β* double heterozygous (+/−) and *ATF6α/β*–double KO (−/−) medaka relative to the expression level of β-actin (n = 3). Each value in WT medaka is set to 1. Data presented are means ± SD. *, P < 0.05; **, P < 0.01.

set as +1) is the binding site of BBF2H7 (Saito et al., 2009a). We found two CRE-like sequences each in medaka *Sec23a* and *Tago1* promoter (Fig. 8 E); however, mutation of these sequences did not affect the response of the respective promoter to medaka BBF2H7(N) (Fig. 8 D, Mut1 and Mut2) or human BBF2H7(N) (Fig. S4, Mut1 and Mut2). The binding site or sites of medaka BBF2H7(N) in *Sec23a* and *Tango1* promoters remain to be determined.

Discussion

We previously showed that ATF6α/β is required for smooth alignment of notochord cells, which synthesize and secrete various extracellular matrix proteins, including type VIII collagen (Ishikawa et al., 2013). Although type VIII collagen is ∼130 nm long (Yamaguchi et al., 1991), it can be folded into a compact structure using multiple breaks consisting of two amino acids within 145 repeats of the triplet amino acids Gly-X-Y (Fig. S1) during transport in standard COPII vesicles (60–80 nm diameter), once folded with the assistance of ER chaperones, whose expression levels are adjusted by ATF6 in accordance with demand.

In this study, we show that the ER membrane–bound transcription factor BBF2H7 is required for the process termed vacuolization of the notochord, which occurs after smooth alignment of notochord cells. In the absence of BBF2H7, type II collagen was not secreted but aggregated, probably in the ER

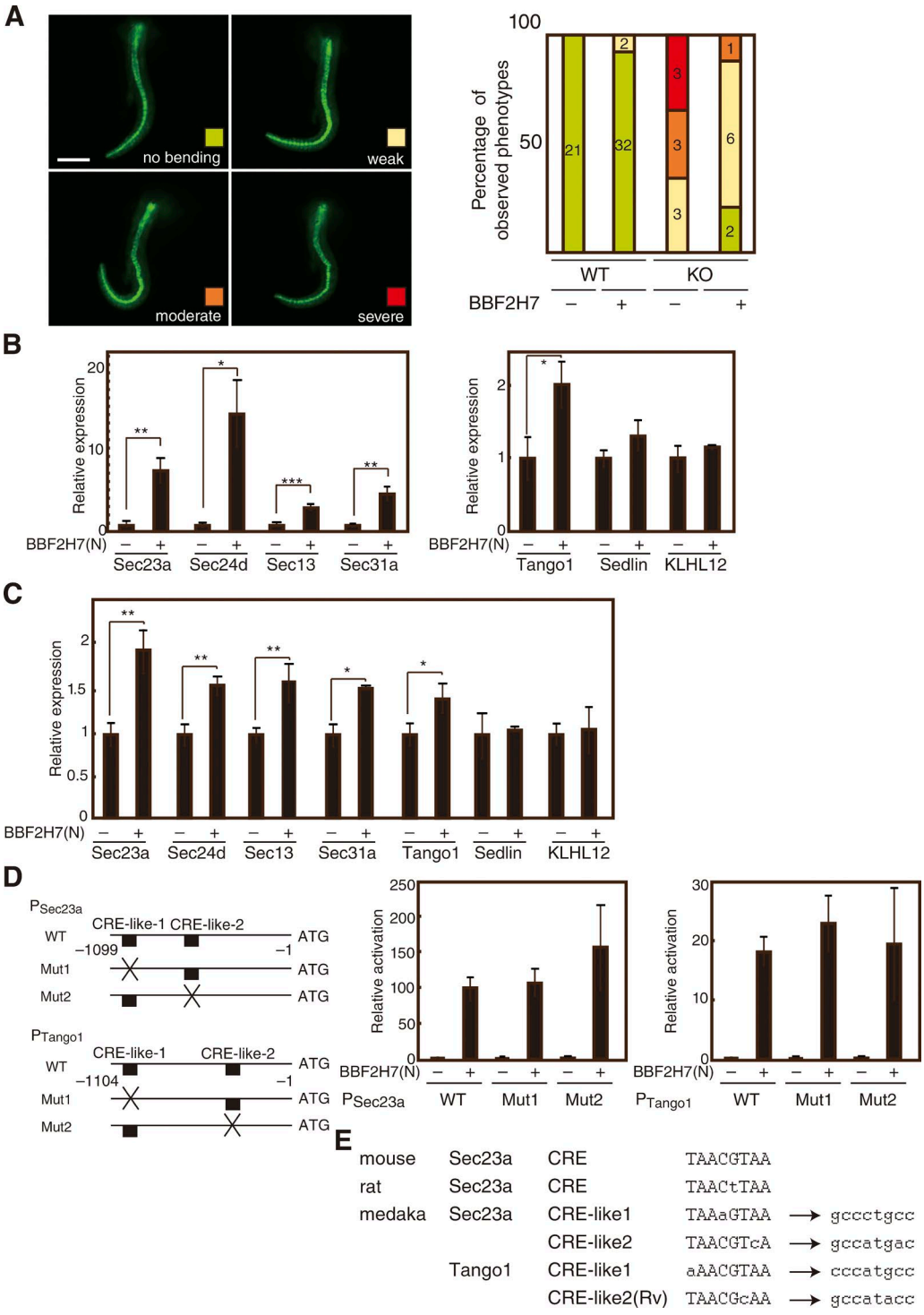

Figure 8. **Enlargement of COPII vesicles by BBF2H7-mediated transcriptional regulation.** (A) Rescue of abnormality during vacuolization of the notochord observed in *BBF2H7*-KO medaka by transient expression (+) of BBF2H7 via microinjection of 100 ng/µl *BBF2H7* mRNA into one cell–stage embryos based on fluorescence microscopic analysis of WT and *BBF2H7*-KO medaka expressing $P_{brachyury}$-*Venus* at stage 27. Embryos were phenotypically classified into four categories, namely no bending (green), weak (yellow), moderate (orange), and severe (red), based on the number and severity of bending, and then genotyped. *n* is indicated in each column. Bar, 250 µm. (B) Quantitative RT-PCR analysis of expression levels of genes involved in the formation of enlarged COPII vesicles relative to the expression level of β-actin in embryos at stage 15 of WT medaka after microinjection (+) of 50 ng/µl *BBF2H7(N)* mRNA into one cell–stage embryos ($n = 3$). Each value in the absence (–) of BBF2H7(N) mRNA injection is set to 1, which also applies to D. (C) Quantitative RT-PCR analysis of expression levels of genes involved in the formation of enlarged COPII vesicles relative to the expression level of GAPDH in human chondrosarcoma-derived chondrocytic cell line HCS-2/8 24 h after transfection (+) of plasmid to express human BBF2H7(N) ($n = 3$). Each value in the absence (–) of BBF2H7(N) transfection is set to 1.*, $P < 0.05$; **, $P < 0.01$; ***, $P < 0.001$. (D) Schematic representation of WT and mutant promoters of the *Sec23* and *Tango1* genes. The translational start site is set as +1. Reporter luciferase assay was performed with (+) or without (–) microinjection of 50 ng/µl medaka *BBF2H7(N)* mRNA, as described in the Luciferase assay section of Materials and methods, and the results are shown on the right. Data presented are means ± SD. (E) Comparison of CRE sequences present in mouse and rat *Sec23a* promoters with CRE-like sequences present in medaka *Sec23a* and *Tango1* promoters. CRE-like sequences were mutated as indicated. Rv, reverse orientation.

of sheath cells. Accordingly, formation of the perinotochordal basement membrane was prevented, resulting in bending and progression defects in the notochord. As type II collagen is 300–400 nm long, it cannot be transported in standard COPII vesicles, even if it is folded with the aid of ATF6-mediated adjustment of ER chaperone expression levels.

The accumulation of type II collagen has been shown in the ER of chondrocytes in *BBF2H7*-KO mice and in the zebrafish *feelgood* mutant (Saito et al., 2009a; Melville et al., 2011). These studies further showed that, among the inner coat components of COPII vesicles, *sec23a* is the target of mouse BBF2H7 and that *sec23a*, *sec23b*, and *sec24d* (but not *sec24c*) are targets of zebrafish BBF2H7. Although interesting, these findings are insufficient to explain the phenotype of *BBF2H7*-KO medaka, because sec23 and sec24 are core components of both standard and enlarged COPII vesicles.

In this study, we show for the first time that BBF2H7 is required for transcriptional regulation of a complete set of genes (*Sec23a*/*24d*/*13*/*31a*, *Tango1*, *Sedlin*, and *KLHL12*) essential for the enlargement of COPII vesicles to accommodate long-chain collagen for export from the ER. Among these, we show that transcription of the *Sec23a*/*24d*/*13*/*31a* and *Tango1* genes is enhanced by transient overexpression of the active form of BBF2H7 in embryos and further show that at least *Sec23a* and *Tango1* are direct targets of BBF2H7 by reporter assays in embryos, although the cis-acting element or elements responsible for this regulation remain to be determined. In contrast, transcription of the *Sedlin* and *KLHL12* genes was not enhanced by transient overexpression of the active form of BBF2H7 in embryos, suggesting that their transcriptional induction may require the presence of a cofactor or cofactors or heterodimerization with other transcription factors expressed in a developmental stage–specific manner. This is because we had to do these experiments in very early stage embryos (stage 15), far earlier than stage 27, when vacuolization of the notochord occurs, because of the apparent toxicity of the active form of BBF2H7 on embryonic development. It is also possible that the chromatin structures of the aforementioned genes change depending on developmental stage. In this connection, transcription of the *Tango1* gene was enhanced by the active form of BBF2H7 in the human chondrosarcoma-derived chondrocytic cell line HCS-2/8, synthesizing and secreting a large amount of type II collagen, but not in the human colorectal carcinoma cell HCT116. In any event, transcriptional regulation of the *Tango1* gene is most important for the enlargement of COPII vesicles because Tango1 initiates enlargement by recognizing the emergence of long-chain collagen in the ER via direct binding. It is interesting to note that only the mRNA encoding SLY1, a partner of Tango1, was down-regulated in *BBF2H7*-KO medaka among various candidate mRNAs.

The UPR is considered to be activated by the accumulation of unfolded/misfolded proteins in the ER and is therefore easily elicited by the addition of chemicals such as tunicamycin (inhibitor of protein *N*-glycosylation), thapsigargin (inhibitor of Ca^{2+} pump in the ER), or dithiothreitol (reducing reagent; Kaufman, 1999). However, these chemicals cause the severe and simultaneous misfolding of many proteins, which often overwhelms the UPR. For example, treatment of the medaka embryo with tunicamycin promptly impaired progression of the notochord even though the major ER chaperone BiP is transcriptionally induced via activation of the UPR (Ishikawa et al., 2013).

In repudiation, we now claim that chemically induced ER stress is too artificial and does not represent what actually occurs within the living organism. Evidencing this, we demonstrate here for the first time that proteins causing physiological ER stress differ depending on developmental stage and that the most appropriate UPR transducer is activated to cope with a specific ER stress, as exemplified in this study by activation of ATF6 for the folding of type VIII collagen during the smooth alignment of notochord cells and of ATF6 and BBF2H7 for the folding and export of type II collagen during vacuolization of notochord cells. See Fig. 9 for a model of these results. Thus, the use of chemically induced ER stress is of limited value in untangling the mechanism of UPR transducers in vivo, and future studies should consider the use of more specific inducers.

Although Mib-Jag1-Notch signaling is certainly a trigger for the differentiation of notochord cells into sheath cells, the signal input by the main actors is not at all sufficient for differentiation. Completion of the vacuolization step definitely relies on BBF2H7-mediated enlargement of COPII vesicles for export of synthesized type II collagen from the ER. We therefore consider that the UPR orchestrates various biological processes by providing backstage support to main actors.

The next critical issue is to unravel the basis for the remarkable ability of the ER in discriminating the difference in the length of synthesized collagen to activate BBF2H7. In particular, it would be intriguing to determine whether BBF2H7 itself recognizes the difference, or whether some other molecules sense the difference and relay the signal to BBF2H7.

Materials and methods

Fish, imaging, TILLING method, and statistical analysis

Medaka southern strain Cab were used as WT fish. Fish were maintained in a recirculating system with a 14:10 h light/dark cycle at 27.5°C. All experiments were performed in accordance with the guidelines and regulations established by the Animal Research Committee of Kyoto University (approval number: H2819). WT fish carrying P_{BiP}-*EGFP* (TG998) or $P_{brachyury}$-*Venus* (TG1005) are available at the National BioResource Project (NBRP Medaka).

Venus or EGFP imaging was performed under a fluorescent stereomicroscope (M205FA) using a GFP3 filter (470/40-nm excitation filter and 525/50-nm barrier filter) or YFP filter (500/520-nm excitation filter and 540/580-emission filter) with a camera (DFX310FX) and acquisition software (Las AF) or under a confocal microscopic system (TCS SP2; Leica Biosystems) using a 63× 1.40 NA objective lens at room temperature.

The missense mutation of BBF2H7 (M1V) was identified from a library of 5,760 mutated male fish of N1 (Taniguchi et al., 2006) by subjecting PCR fragments amplified from this library using the primer sets 5′-ATCCAATATCTAAACGACGGAAGAA-3′ and 5′-TCACTT GTCGACACAGTGG-3′ to high-resolution melting curve analysis (Ishikawa et al., 2010) and subsequent sequencing.

Statistical analysis was conducted using Student's *t* test. *, $P<0.05$; **, $P < 0.01$; and ***, $P < 0.001$ for all figures.

Construction of plasmids

Recombinant DNA techniques were performed according to standard procedures (Sambrook et al., 1989), and the integrity of all constructed plasmids was confirmed by extensive sequencing analyses. Site-directed mutagenesis was performed using Dpn I.

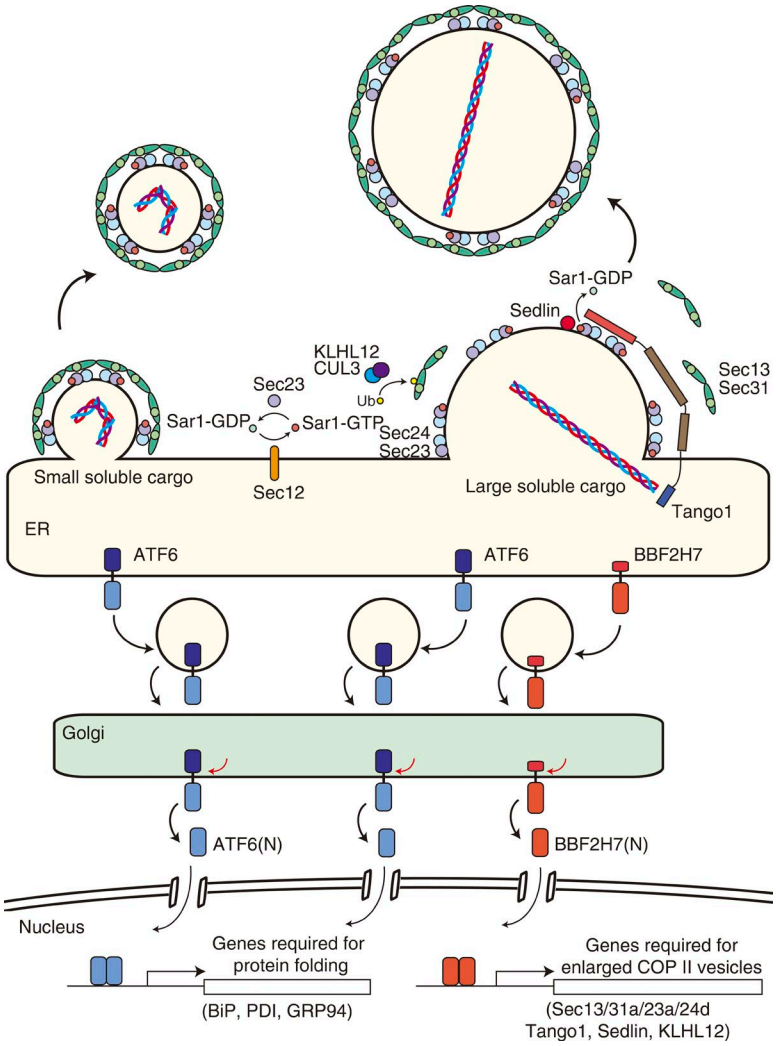

Figure 9. **Activation of the most appropriate UPR transducer to cope with a specific ER stress.** ATF6 is required for smooth alignment of notochord cells, which synthesize and secrete various extracellular matrix proteins, including type VIII collagen. Because type VIII collagen can be folded into a compact structure, it can be transported in standard COPII vesicles (60–80 nm diameter) once folded with the assistance of ER chaperones, whose expression levels are adjusted by ATF6 in accordance with demand. BBF2H7 is required for the process, termed vacuolization of the notochord, which occurs after the differentiation of notochord cells into sheath cells. As type II collagen synthesized and secreted by sheath cells is 300–400 nm long, it cannot be transported in standard COPII vesicles, even if it is folded with the aid of ATF6-mediated adjustment of ER chaperone expression levels. BBF2H7 regulates transcription of a complete set of genes (*Sec23a/24d/13/31a*, *Tango1*, *Sedlin*, and *KLHL12*) essential for the enlargement of COPII vesicles to accommodate type II collagen for export from the ER. Ub, ubiquitin.

Full-length and nuclear forms of medaka BBF2H7 were amplified from a medaka 1-dph cDNA library using the primer pairs 5′-TTCGAATTCGCCACCATGGAGATCCTGGACAGCAG-3′ and 5′-AGTTCTAGATTAGGACGTCTCGTTGACGG-3′, and 5′-TTCGAATTCGCCACCATGGAGATCCTGGACAGCAG-3′ and 5′-AGTTCTAGATTAGGTCCCGGCCACCCGGCAGG-3′, respectively, and then were subcloned between the EcoRI and XbaI sites of pCS2 (Rupp et al., 1994) for in vitro transcription. The nuclear form of human BBF2H7 was amplified from an HCT116 cell cDNA library using the primer pair 5′-CCCGAATTCCCATGGAGGTGCTGGAGAGCG-3′ and 5′-GAGAGATCTAGGTGCCAGTCTGCGTGCCAG-3′ and then was subcloned between the EcoRI and BglII sites of pCMV-myc (Takara Bio Inc.).

Medaka *Sec23a* and *Tango1* promoters were amplified from medaka genomic DNA using the primer pairs 5′-CATAGATCTGCACAAGCGGGATCATGTGCT-3′ and 5′-TCCTCGTTCTGAGCGATGTACTCCGCGAAG-3′, and 5′-TTAAGATCTTATCTTACGGAAATAGGTTTT-3′ and 5′-CTGCCATGGTGGCAGTTAGTGTAGCCGGAC-3′, respectively, and then were subcloned between the BglII and NcoI sites of pGL4-basic (Promega).

Genotyping

Embryos or hatched fish were suspended in 50 µl lysis buffer (10 mM NaOH and 0.2 mM EDTA), boiled for 5 min, and then neutralized by the addition of 50 µl of 40 mM Tris/HCl, pH 8.0. The DNA fragment containing the mutation site (M1V) was amplified by PCR directly from lysates using the aforementioned primers, and amplified fragments were directly sequenced or digested with NlaIII.

Alcian blue staining

Hatched fish were fixed in 4% paraformaldehyde and 1% NaOH in PBS, washed with PBST (0.1% Tween-20 in PBS) three times, stained with 0.1% alcian blue in 70% ethanol and 30% acetic acid, and then washed with 100% ethanol three times followed by washing with 95% ethanol, 75% ethanol, 50% ethanol, 25% ethanol, and PBST. Stained fish were bleached in 3% hydrogen peroxide in 1% KOH, washed with PBST three times, and treated with trypsin to digest tissues other than bones.

Alizarin red staining

Hatched fishes were fixed in 4% paraformaldehyde and 1% NaOH in PBS, washed with PBST three times, and stained with 4% alizarin red S in 0.5% KOH for 5 min, followed by extensive washing with 0.5% KOH.

Construction of transgenic line–expressing P_{BBF2H7}-*Venus* or $P_{brachyury}$-*Venus*

To generate fluorescent reporter constructs, two fosmid vector clones containing the *BBF2H7* (GOLWFno460_f02) or *brachyury* (GOLWFno430_o13) gene were obtained from K. Naruse of the National BioResource Project (NBRP Medaka) at National Institute for Basic Biology, Okazaki, Japan. Two-step homologous recombination was

performed as described previously (Ishikawa et al., 2011) using 5′-cag aggacgtgggggaaaaatatccaatatctaaacgacggaagaagtcATGGTGAGC AAGGGCGAGGA-3′ and 5′-ctgatcagcagatcctgatcgatcacttgtcgacac agtggatcactcacACCAGTTGGTGATTTTGAAC-3′ as forward and reverse primers, respectively, for P_{BBF2H7}-*Venus,* and 5′-cgtttcggatt cagtccctggatttgtcttcgagcgcctcacctggaaatATGGTGAGCAAGGGC GAGGA-3′ and 5′-gcacgctgactgagagacggcctcgccgcgcgctgctgctgtcc acctacACCAGTTGGTGATTTTGAAC-3′ as forward and reverse primers, respectively, for $P_{brachyury}$-*Venus*. Lowercase letters correspond to the 5′ and 3′ sequences of each first exon. Uppercase letters of the forward and reverse primers correspond to the 5′ sequences of *Venus* and the 3′ sequences of the kanamycin-resistant gene, respectively. Each fosmid construct was injected into one cell–stage embryos as described previously (Ishikawa et al., 2011).

Immunofluorescence

Embryos were fixed in 4% paraformaldehyde in PBS for 1 h at room temperature, washed with PBS, fixed again with 100% methanol overnight at 4°C, and then washed with 75% methanol plus 25% PBST, 50% methanol plus 50% PBST, 25% methanol plus 75% PBST, and 100% PBST. Fixed embryos were permeabilized by incubation with 0.1 mg/ml proteinase K in PBSX (0.1% Triton X-100 in PBS) for 15 min at room temperature and then washed with PBS DX (1% DMSO and 0.3% Triton X-100 in PBS) three times. Permeabilized embryos were blocked in blocking solution (2% fetal bovine serum and 2 mg/ml BSA in PBSX) for 15 min at room temperature, reacted with mouse anti–type II collagen antibody (Thermo Fisher Scientific) and rabbit anti-calnexin antibody (ADI-SPA-865; Enzo Life Sciences) in blocking solution for two nights at 4°C, washed five times with PBSDX, reacted with goat anti–mouse IgG heavy and light chains (Alexa Flour 568) and goat anti-rabbit IgG heavy and light chains (Alexa Flour 488; Invitrogen) for 1 h at room temperature, and then washed with PBST.

Electron microscopy

Embryos were fixed with 2% paraformaldehyde and 2.5% glutaraldehyde in 0.1 M phosphate buffer, pH 7.4. Their egg envelopes were removed and they were further fixed overnight at room temperature. They were washed with PBS, washed with 10% sucrose in Hepes buffer (30 mM Hepes, 100 mM NaCl, and 2 mM $CaCl_2$, pH 7.4), and post-fixed in 1% osmium tetroxide in Hepes buffer for 1 h on ice. They were washed several times with distilled water, stained with 0.5% uranyl acetate in distilled water overnight, dehydrated, embedded as described previously (Harada et al., 1990), and analyzed using a transmission electron microscope (H-7650; Hitachi).

Quantitative RT-PCR

Total RNA was extracted from embryos or the notochord (enzymatically removed by pancreatin treatment) at 2 dpf by the acid guanidinium/phenol/chloroform method using isogen (Nippon Gene). For quantitative RT-PCR analysis, total RNA was purified by ethanol precipitation, reverse transcribed using an oligonucleotide deoxythymine primer, and then subjected to a StepOne Real-Time PCR System (Applied Biosystems) using the primers described in Table S1.

Microinjection of mRNA synthesized in vitro

BBH2H7 mRNA or *BBF2H7(N)* mRNA was transcribed in vitro from full-length or truncated *BBF2H7* cDNA with a mMESSAGE mMACHINE kit (Ambion), purified by RNeasy MinElute (QIAGEN), dissolved in 0.5× Yamamoto's buffer, 0.5× I-SceI buffer, and 0.05% phenol red at the concentration of 100 or 50 ng/µl, and then microinjected into one cell–stage embryos using a FemtoJet (Eppendorf).

Cell culture

The human chondrosarcoma-derived chondrocytic cell line HCS-2/8 (Takigawa et al., 1989) and the human colorectal carcinoma cell HCT116 (CCL-247; ATCC) were cultured in DMEM (glucose 4.5 g/liter) supplemented with 10% fetal bovine serum, 2 mM glutamine, and antibiotics (100 U/ml penicillin and 100 µg/ml streptomycin) at 37°C in a humidified 5% CO_2/95% air atmosphere and were transfected using 10 µg PEI-MAX and 1 µg DNA.

Luciferase assay

Several one cell–stage embryos, into which respective firefly luciferase reporter plasmid (7 ng/µl) and renilla luciferase reference plasmid (3 ng/µl) were microinjected with or without medaka or human *BBF2H7(N)* mRNA (50 ng/µl), were grown until stage 15 and then lysed with 50 µl/embryo lysis buffer. Luciferase activities were measured using the Picagene Dual Assay kit (Toyo Ink) and a TriStar LB941 Multimode Microplate Reader (Berthold).

Online supplemental materials

Fig. S1 shows a comparison of type VIII collagen with type II collagen. Fig. S2 gives an outline of the construction of a transgenic line expressing $P_{brachyury}$-Venus. Fig. S3 shows the effect of overexpression of BBF2H7(N) on transcription in HCT116 cells. Fig. S4 shows the effect of overexpression of human BBF2H7(N) on WT and mutant promoters of medaka *Sec23a* and *Tango1* genes. Table S1 shows sequences of primers used for quantitative RT-PCR.

Acknowledgments

We thank Ms. Kaoru Miyagawa and Ms. Yuki Okada for their technical and secretarial assistance.

This work was financially supported in part by grants from the Ministry of Education, Culture, Sports, Science and Technology of Japan (26291040 and 17H01432 to K. Mori and 15K18529 and 17K15116 to T. Ishikawa).

The authors declare no competing financial interests.

Author contributions: T. Ishikawa, T. Toyama, Y. Nakamura, K. Tamada, H. Shimizu, S. Ninagawa, and T. Okada conducted the experiments. A. Harada conducted electron microscopic analysis. Y. Kamei, T. Ishikawa-Fujiwara, and T. Todo collaborated for the identification of *BBF2H7*-KO medaka. E. Aoyama and M. Takigawa collaborated for analysis of the human chondrosarcoma-derived chondrocytic cell line HCS-2/8. K. Mori designed the experiments and wrote the paper.

Submitted: 22 September 2016
Revised: 5 March 2017
Accepted: 12 April 2017

References

Asada, R., S. Kanemoto, S. Kondo, A. Saito, and K. Imaizumi. 2011. The signalling from endoplasmic reticulum-resident bZIP transcription factors involved in diverse cellular physiology. *J. Biochem.* 149:507–518. http://dx.doi.org/10.1093/jb/mvr041

Bertolotti, A., X. Wang, I. Novoa, R. Jungreis, K. Schlessinger, J.H. Cho, A.B. West, and D. Ron. 2001. Increased sensitivity to dextran sodium sulfate colitis in IRE1β-deficient mice. *J. Clin. Invest.* 107:585–593. http://dx.doi.org/10.1172/JCI11476

Cox, J.S., C.E. Shamu, and P. Walter. 1993. Transcriptional induction of genes encoding endoplasmic reticulum resident proteins requires a transmembrane protein kinase. *Cell.* 73:1197–1206. http://dx.doi.org/10.1016/0092-8674(93)90648-A

Dietrich, S., F.R. Schubert, and P. Gruss. 1993. Altered *Pax* gene expression in murine notochord mutants: the notochord is required to initiate and

maintain ventral identity in the somite. *Mech. Dev.* 44:189–207. http://dx.doi.org/10.1016/0925-4773(93)90067-8

Harada, A., K. Sobue, and N. Hirokawa. 1990. Developmental changes of synapsin I subcellular localization in rat cerebellar neurons. *Cell Struct. Funct.* 15:329–342. http://dx.doi.org/10.1247/csf.15.329

Harding, H.P., H. Zeng, Y. Zhang, R. Jungries, P. Chung, H. Plesken, D.D. Sabatini, and D. Ron. 2001. Diabetes mellitus and exocrine pancreatic dysfunction in *perk−/−* mice reveals a role for translational control in secretory cell survival. *Mol. Cell.* 7:1153–1163. http://dx.doi.org/10.1016/S1097-2765(01)00264-7

Hollien, J., and J.S. Weissman. 2006. Decay of endoplasmic reticulum-localized mRNAs during the unfolded protein response. *Science.* 313:104–107. http://dx.doi.org/10.1126/science.1129631

Hubbard, T., D. Barker, E. Birney, G. Cameron, Y. Chen, L. Clark, T. Cox, J. Cuff, V. Curwen, T. Down, et al. 2002. The Ensembl genome database project. *Nucleic Acids Res.* 30:38–41.

Ishikawa, T., Y. Kamei, S. Otozai, J. Kim, A. Sato, Y. Kuwahara, M. Tanaka, T. Deguchi, H. Inohara, T. Tsujimura, and T. Todo. 2010. High-resolution melting curve analysis for rapid detection of mutations in a Medaka TIL LING library. *BMC Mol. Biol.* 11:70. http://dx.doi.org/10.1186/1471-2199-11-70

Ishikawa, T., Y. Taniguchi, T. Okada, S. Takeda, and K. Mori. 2011. Vertebrate unfolded protein response: Mammalian signaling pathways are conserved in medaka fish. *Cell Struct. Funct.* 36:247–259. http://dx.doi.org/10.1247/csf.11036

Ishikawa, T., T. Okada, T. Ishikawa-Fujiwara, T. Todo, Y. Kamei, S. Shigenobu, M. Tanaka, T.L. Saito, J. Yoshimura, S. Morishita, et al. 2013. ATF6α/β-mediated adjustment of ER chaperone levels is essential for development of the notochord in medaka fish. *Mol. Biol. Cell.* 24:1387–1395. http://dx.doi.org/10.1091/mbc.E12-11-0830

Jin, L., K.B. Pahuja, K.E. Wickliffe, A. Gorur, C. Baumgärtel, R. Schekman, and M. Rape. 2012. Ubiquitin-dependent regulation of COPII coat size and function. *Nature.* 482:495–500. http://dx.doi.org/10.1038/nature10822

Kaufman, R.J. 1999. Stress signaling from the lumen of the endoplasmic reticulum: coordination of gene transcriptional and translational controls. *Genes Dev.* 13:1211–1233. http://dx.doi.org/10.1101/gad.13.10.1211

Kondo, S., A. Saito, S. Hino, T. Murakami, M. Ogata, S. Kanemoto, S. Nara, A. Yamashita, K. Yoshinaga, H. Hara, and K. Imaizumi. 2007. BBF2H7, a novel transmembrane bZIP transcription factor, is a new type of endoplasmic reticulum stress transducer. *Mol. Cell. Biol.* 27:1716–1729. http://dx.doi.org/10.1128/MCB.01552-06

Lerner, D.W., D. McCoy, A.J. Isabella, A.P. Mahowald, G.F. Gerlach, T.A. Chaudhry, and S. Horne-Badovinac. 2013. A Rab10-dependent mechanism for polarized basement membrane secretion during organ morphogenesis. *Dev. Cell.* 24:159–168. http://dx.doi.org/10.1016/j.devcel.2012.12.005

Malhotra, V., and P. Erlmann. 2015. The pathway of collagen secretion. *Annu. Rev. Cell Dev. Biol.* 31:109–124. http://dx.doi.org/10.1146/annurev-cellbio-100913-013002

McGourty, C.A., D. Akopian, C. Walsh, A. Gorur, A. Werner, R. Schekman, D. Bautista, and M. Rape. 2016. Regulation of the CUL3 ubiquitin ligase by a calcium-dependent co-adaptor. *Cell.* 167:525–538.e14. http://dx.doi.org/10.1016/j.cell.2016.09.026

Melville, D.B., M. Montero-Balaguer, D.S. Levic, K. Bradley, J.R. Smith, A.K. Hatzopoulos, and E.W. Knapik. 2011. The *feelgood* mutation in zebrafish dysregulates COPII-dependent secretion of select extracellular matrix proteins in skeletal morphogenesis. *Dis. Model. Mech.* 4:763–776. http://dx.doi.org/10.1242/dmm.007625

Mori, K. 2000. Tripartite management of unfolded proteins in the endoplasmic reticulum. *Cell.* 101:451–454. http://dx.doi.org/10.1016/S0092-8674(00)80855-7

Mori, K., W. Ma, M.J. Gething, and J. Sambrook. 1993. A transmembrane protein with a cdc2+/CDC28-related kinase activity is required for signaling from the ER to the nucleus. *Cell.* 74:743–756. http://dx.doi.org/10.1016/0092-8674(93)90521-Q

Nogueira, C., P. Erlmann, J. Villeneuve, A.J. Santos, E. Martínez-Alonso, J.A. Martínez-Menárguez, and V. Malhotra. 2014. SLY1 and Syntaxin 18 specify a distinct pathway for procollagen VII export from the endoplasmic reticulum. *eLife.* 3:e02784. http://dx.doi.org/10.7554/eLife.02784

Rupp, R.A., L. Snider, and H. Weintraub. 1994. Xenopus embryos regulate the nuclear localization of XMyoD. *Genes Dev.* 8:1311–1323. http://dx.doi.org/10.1101/gad.8.11.1311

Saito, A., S. Hino, T. Murakami, S. Kanemoto, S. Kondo, M. Saitoh, R. Nishimura, T. Yoneda, T. Furuichi, S. Ikegawa, et al. 2009a. Regulation of endoplasmic reticulum stress response by a BBF2H7-mediated Sec23a pathway is essential for chondrogenesis. *Nat. Cell Biol.* 11:1197–1204. http://dx.doi.org/10.1038/ncb1962

Saito, K., M. Chen, F. Bard, S. Chen, H. Zhou, D. Woodley, R. Polischuk, R. Schekman, and V. Malhotra. 2009b. TANGO1 facilitates cargo loading at endoplasmic reticulum exit sites. *Cell.* 136:891–902. http://dx.doi.org/10.1016/j.cell.2008.12.025

Saito, K., K. Yamashiro, Y. Ichikawa, P. Erlmann, K. Kontani, V. Malhotra, and T. Katada. 2011. cTAGE5 mediates collagen secretion through interaction with TANGO1 at endoplasmic reticulum exit sites. *Mol. Biol. Cell.* 22:2301–2308. http://dx.doi.org/10.1091/mbc.E11-02-0143

Sambrook, J., E.F. Fritsch, and T. Maniatis. 1989. Molecular cloning: A laboratory manual. Cold Spring Harbor Laboratory Press, Cold Spring Harbor, New York.

Schulte-Merker, S., R.K. Ho, B.G. Herrmann, and C. Nüsslein-Volhard. 1992. The protein product of the zebrafish homologue of the mouse T gene is expressed in nuclei of the germ ring and the notochord of the early embryo. *Development.* 116:1021–1032.

Shen, X., R.E. Ellis, K. Sakaki, and R.J. Kaufman. 2005. Genetic interactions due to constitutive and inducible gene regulation mediated by the unfolded protein response in *C. elegans. PLoS Genet.* 1:355–368. http://dx.doi.org/10.1371/journal.pgen.0010037

Stemple, D.L. 2005. Structure and function of the notochord: an essential organ for chordate development. *Development.* 132:2503–2512. http://dx.doi.org/10.1242/dev.01812

Takigawa, M., K. Tajima, H.O. Pan, M. Enomoto, A. Kinoshita, F. Suzuki, Y. Takano, and Y. Mori. 1989. Establishment of a clonal human chondrosarcoma cell line with cartilage phenotypes. *Cancer Res.* 49:3996–4002.

Taniguchi, Y., S. Takeda, M. Furutani-Seiki, Y. Kamei, T. Todo, T. Sasado, T. Deguchi, H. Kondoh, J. Mudde, M. Yamazoe, et al. 2006. Generation of medaka gene knockout models by target-selected mutagenesis. *Genome Biol.* 7:R116. http://dx.doi.org/10.1186/gb-2006-7-12-r116

Urano, F., X. Wang, A. Bertolotti, Y. Zhang, P. Chung, H.P. Harding, and D. Ron. 2000. Coupling of stress in the ER to activation of JNK protein kinases by transmembrane protein kinase IRE1. *Science.* 287:664–666. http://dx.doi.org/10.1126/science.287.5453.664

Venditti, R., T. Scanu, M. Santoro, G. Di Tullio, A. Spaar, R. Gaibisso, G.V. Beznoussenko, A.A. Mironov, A. Mironov Jr., L. Zelante, et al. 2012. Sedlin controls the ER export of procollagen by regulating the Sar1 cycle. *Science.* 337:1668–1672. http://dx.doi.org/10.1126/science.1224947

Walter, P., and D. Ron. 2011. The unfolded protein response: From stress pathway to homeostatic regulation. *Science.* 334:1081–1086. http://dx.doi.org/10.1126/science.1209038

Wilkinson, D.G., S. Bhatt, and B.G. Herrmann. 1990. Expression pattern of the mouse T gene and its role in mesoderm formation. *Nature.* 343:657–659. http://dx.doi.org/10.1038/343657a0

Yamaguchi, N., R. Mayne, and Y. Ninomiya. 1991. The α1 (VIII) collagen gene is homologous to the α1 (X) collagen gene and contains a large exon encoding the entire triple helical and carboxyl-terminal non-triple helical domains of the α1 (VIII) polypeptide. *J. Biol. Chem.* 266:4508–4513.

Yamamoto, K., T. Sato, T. Matsui, M. Sato, T. Okada, H. Yoshida, A. Harada, and K. Mori. 2007. Transcriptional induction of mammalian ER quality control proteins is mediated by single or combined action of ATF6α and XBP1. *Dev. Cell.* 13:365–376. http://dx.doi.org/10.1016/j.devcel.2007.07.018

Yamamoto, M., R. Morita, T. Mizoguchi, H. Matsuo, M. Isoda, T. Ishitani, A.B. Chitnis, K. Matsumoto, J.G. Crump, K. Hozumi, et al. 2010. Mib-Jag1-Notch signalling regulates patterning and structural roles of the notochord by controlling cell-fate decisions. *Development.* 137:2527–2537. http://dx.doi.org/10.1242/dev.051011